Device

Article

A clickable embroidered triboelectric sensor for smart fabric

Graphical abstract

Authors

Yu Chen, Yali Ling, Yiduo Yang, ..., Bao Yang, Xiaoming Tao, Rong Yin

Correspondence

byang20210415@scut.edu.cn (B.Y.), xiao-ming.tao@polyu.edu.hk (X.T.), ryin@ncsu.edu (R.Y.)

In brief

This work demonstrates an embroidery sensor for human-machine interaction. Based on conventional embroidery and special needle stiches, a 3D embroidery structure was achieved. This embroidery sensor can be integrated into normal fabrics as a clickable control. With the assistance of machine learning, we demonstrated the sensor's capability to be used for apps and game control as well as interaction with other devices.

Highlights

- A flexible 3D TENG embroidery sensor for human-machine interface is presented
- A microchip-embedded machine learning model was used for signal recognition
- Dual-channel embroidery sensor with different "gaps" was developed
- A sensing array can be constructed using multiple embroidery sensors

2 Explore
Early prototypes with exciting performance and new methodology

Chen et al., 2024, Device 2, 100355
April 19, 2024
https://doi.org/10.1016/j.device.2024.100355

CellPress

Device

CellPress
OPEN ACCESS

Article

A clickable embroidered triboelectric sensor for smart fabric

Yu Chen,[1] Yali Ling,[1] Yiduo Yang,[1] Zihao Wang,[2] Yang Liu,[1] Wei Gao,[1] Bao Yang,[2,*] Xiaoming Tao,[3,*] and Rong Yin[1,4,*]
[1]Textile Engineering, Chemistry and Science, Wilson College of Textiles, North Carolina State University, Raleigh, NC 27695, USA
[2]School of Civil Engineering and Transportation, South China University of Technology, Guangzhou 510640, China
[3]School of Textiles and Clothing, The Hong Kong Polytechnic University, Hong Kong 999077, China
[4]Lead contact
*Correspondence: byang20210415@scut.edu.cn (B.Y.), xiao-ming.tao@polyu.edu.hk (X.T.), ryin@ncsu.edu (R.Y.)
https://doi.org/10.1016/j.device.2024.100355

THE BIGGER PICTURE Most interactive devices are constructed from rigid materials that contrast with the soft and comfortable texture of textiles. Smart textiles, harnessing the potential of flexible electronic technology, offer a promising avenue for the development of comfortable wearable interfaces. However, most flexible electronic devices often still differ from traditional textiles in structure and construction, hindering their integration and scalability. Here, we present an embroidery-based sensor that can achieve touch interaction. By integrating two triboelectric yarns with conventional fabric using a 3D embroidery pattern, a stable triboelectric signal output is achieved. Coupled with machine learning, the embroidery sensor can recognize simple finger gestures for control interfaces. Multiple embroidery sensors can be integrated onto a single piece of fabric in a grid formation for enabling more complicated sensing applications and control interfaces.

SUMMARY

Textile-based human-machine interfaces need to seamlessly integrate electronics with conventional fabrics. Here, we present an embroidery-based device that transforms conventional fabric into a "clickable" button. The device is realized through the integration of dual triboelectric yarns using an embroidery pattern that enables a 3D structure. The design can be customized and optimized by adjusting the gaps between the triboelectric yarns for the needed triboelectric output and other performance metrics, such as consistent contact and separation for the clicking mechanism. Machine learning algorithms are used for signal identification of a diverse range of pressing and swiping gestures on the embroidered device.

INTRODUCTION

Textiles have woven their way through the fabric of human history, driving inventions for their manufacturing, such as the loom and the shuttle, and for their applications, such as different weaving patterns for converting 1D threads into 2D (e.g., rugs) and 3D structures (e.g., baskets).[1–3] Smart textiles represent an intersection where traditional textiles meet modern electronics, embodying capabilities like sensing,[4–8] actuation,[9,10] and human-machine interaction[11,12] while maintaining the comfort and familiarity of fabric.[13,14] This integration has opened a new realm of possibilities in various sectors, including in healthcare for patient monitoring, in sports for performance enhancement, in fashion for interactive clothing, and in the military for improved safety and communications.[15–19]

Textile-based human-machine interfaces manifest in diverse forms, such as gloves,[20,21] wristbands,[22,23] patches,[24–27] and ropes.[28,29] Among these, triboelectric nanogenerator (TENG)-based sensors have gained prominence in wearable sensor design due to their simple design, high sensitivity, and self-powering capabilities.[30] Although these sensors are crafted from flexible materials and utilize textile structures, most are standalone devices and do not integrate well with conventional apparel.[31,32] Those that can be warp knitted or braided typically feature a multilayered structure and larger dimensions with limited flexibility and breathability.[33] In addition, existing textile-based TENG sensors tend to operate in a single-electrode mode, which poses difficulties in achieving stable sensing due to the uncertainties in contact materials,[34–36] and long-term stable contact and separation between flexible materials in textile-based sensors to generate reliable signals remains a challenge. The output signal is also sensitive to environmental

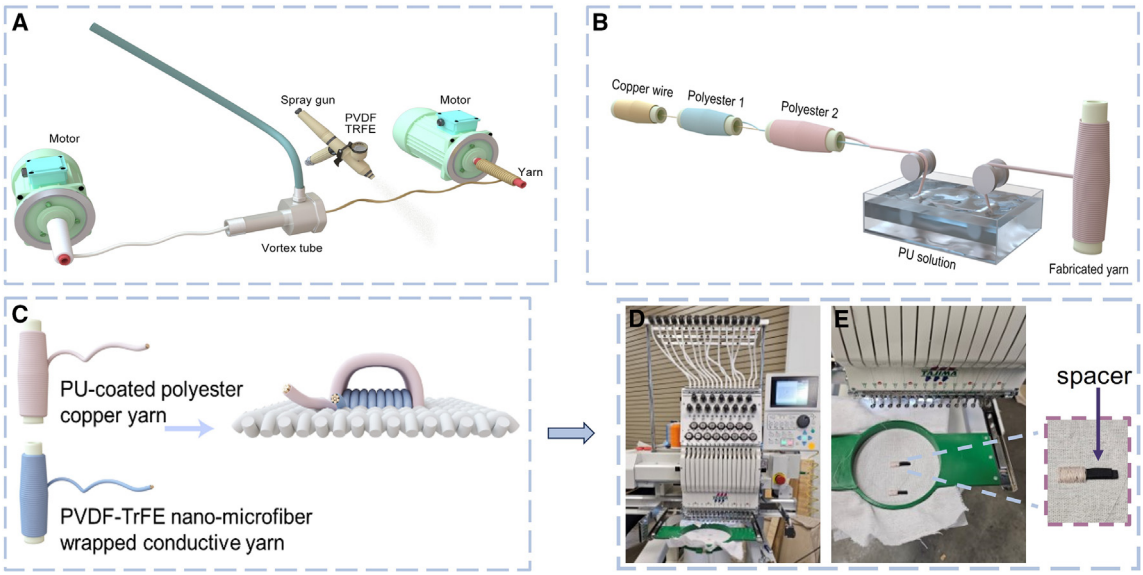

Figure 1. Design and fabrication of the TENG embroidered sensor and interactive system

(A) Schematic of continuous manufacture of PVDF-TrFE nano-microfiber core-sheath conductive yarn with an airflow-driven system.

(B) Schematic of continuous manufacture of PU-coated polyester-copper yarn.

(C) Schematic.

(D) Photo of the electronic automatic embroidery machine.

(E) Modified embroidery method with a spacer.

conditions and fluctuates based on the variability in touch input, posing challenges for more complex (i.e., non-binary) signal recognition and control. Therefore, a strategy that simultaneously integrates sensors with traditional textiles to enable complex signal recognition and control under various scenarios while preserving the inherent qualities of textiles is highly desirable.

Here, we introduce a "clickable" self-powered embroidered sensor. Traditional embroidery, characterized by 2D planar structures and single stitches, is primarily employed for pattern design. Previous research has explored using embroidery patterns and TENG yarns for making single-electrode sensors, but the output signal is highly dependent on external materials.[32,34,37–39] To address this limitation, we utilize various embroidery stitches and incorporate spacers during the embroidering process to achieve 3D embroidery structures. Utilizing polyvinylidene fluoride-trifluoroethylene (PVDF-TrFE) nano-microfiber-wrapped conductive yarn and polyurethane (PU)-coated polyester-copper yarn, we adopted different embroidery techniques to create 3D embroidery structures that can be seamlessly integrated into traditional textiles. The design can be optimized to maximize triboelectric output by adjusting the gaps between the triboelectric yarns and to facilitate stable contact and separation.

The embroidered sensor can be used to input a diverse range of gestures. We implemented machine learning algorithms for signal identification in a series of demonstrations.

RESULTS AND DISCUSSION

Yarn fabrication and system design

The functional device contains two main components: a microchip for signal collection and processing and data transmission and an embroidery pressure sensor. The preparation of the pressure sensor involves two main steps. First, two conductive yarns are prepared using two different triboelectric materials: PVDF-TrFE, a triboelectric negatively charged material due to its fluorine group (-F), and PU, a triboelectric positively charged material due to its amide group (-CONH). These yarns are then embroidered with varying structures to optimize triboelectric performance. Our previous study detailed the preparation of the PVDF-TrFE yarn using an air-driven system (Figures 1A and S1A), which produces PVDF-TrFE nano-microfibers through solution blow spinning that are then wound around silver-plated nylon conductive yarn using a vortex tube.[40] Here, we adopted the procedure to produce PU-coated polyester-copper yarn by winding two strands of polyester fiber on copper wire, first using the Z twist and then again using the S twist, followed by the application of a PU coating (Figures 1B and S1B). These triboelectric yarns are then integrated into conventional textile fabrics using embroidery machines (Figure 1C). The integration employs an embroidery design that optimizes triboelectric output and tactile sensation; the details will be explored in a subsequent section (Figures 1D and 1E).

Characterization of the single embroidered sensor

Scanning electron microscopy (SEM) images of the PU-coated polyester-copper yarn and the PVDF-TrFE nano-microfibers core-sheath conductive yarn are shown in Figures 2A and 2B. In comparison with PVDF-TrFE nano-microfiber conductive yarn, the double-layer polyester and PU coating is stronger (Figure 2C). The PVDF-TrFE nano-microfiber-wrapped conductive yarn is both lighter and more flexible compared with PU-coated

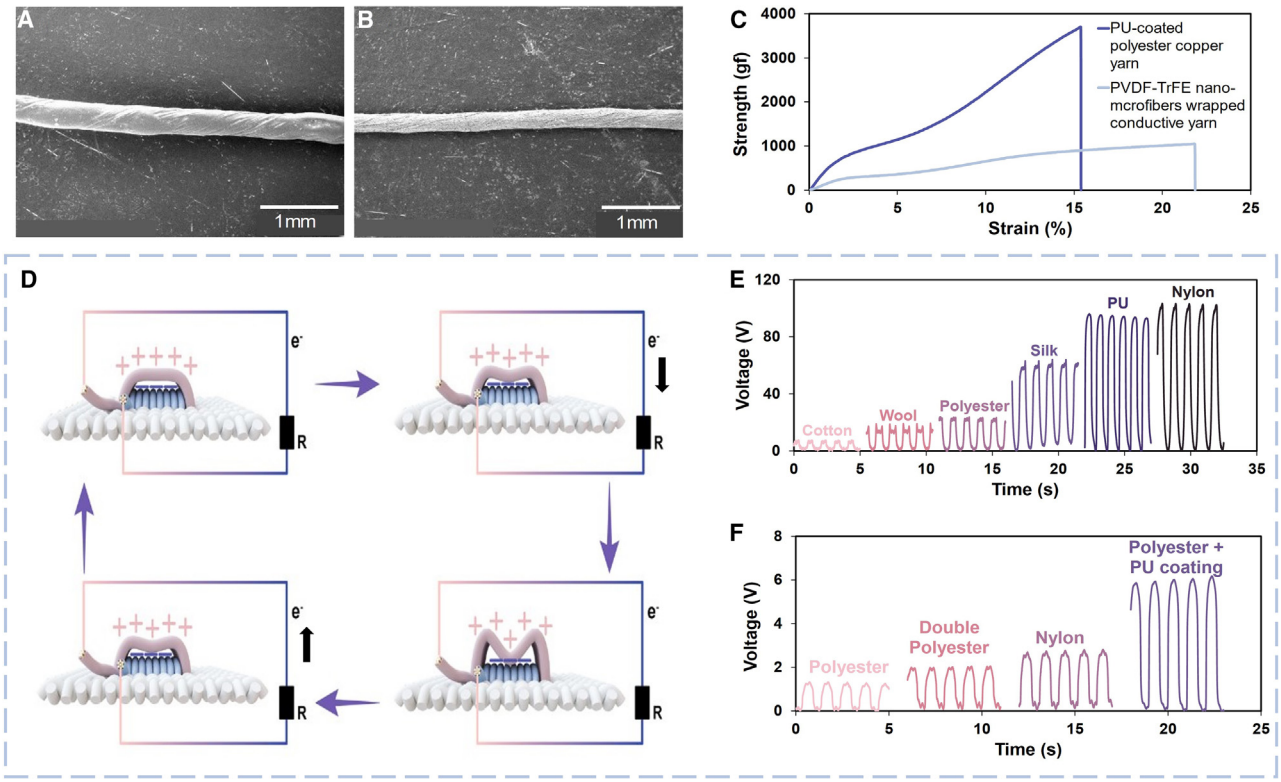

Figure 2. Design and characterization of the TENG embroidered sensor

(A and B) SEM images of (A) PU-coated polyester-copper yarn and (B) PVDF-TrFE nano-microfiber core-sheath conductive yarn.

(C) Tensile properties of PU-coated polyester-copper yarn and PVDF-TrFE nano-microfiber core-sheath conductive yarn.

(D) Structure and working principle of the double-layer embroidered TENG.

(E) Triboelectric performance of PVDF-TrFE nano-microfiber fabric with different textile materials.

(F) Open-circuit voltage of four different wrapping methods and materials with PVDF-TrFE nano-microfiber yarn.

conductive yarn, which makes it more suitable to be used with straight stitches (fitted on the fabric) (Table S1).

A schematic of the double-layer embroidered TENG is shown in Figure 2D. When pressure is applied, the top layer of PU-coated conductive makes contact with the bottom layer of PVDF-TrFE-wrapped conductive yarn, leading to electron exchange that results in the PU layer becoming positively charged and the PVDF layer negatively charged. Upon separation, the electrodes of both layers generate corresponding induced charges to compensate for the charge loss. These charges create a current (~0.3 μA short-circuit current) through the external circuit, generating a triboelectric signal. The PVDF-TrFE nano-microfiber, with its large aspect ratio and high specific surface area, exhibits strong triboelectric properties when it comes into contact with nylon and PU, producing an open-circuit voltage of nearly 100 V (Figure 2E). To protect the delicate PVDF-TrFE nano-microfiber and the conductive silver coating, we opted to use it as the triboelectric yarn for the bottom layer, which is embroidered onto the base fabric using a "straight" stitching pattern. For the top layer, we experimented with four different types of wrapped-copper wires as the triboelectrically positive yarn to test with PVDF-TrFE nano-microfiber-wrapped conductive yarn, which included single-layer polyester copper yarn, double-layer polyester copper yarn, double-layer nylon copper yarn, and PU-coated polyester-copper yarn. The results showed that the PU-coated polyester-copper yarn demonstrates the highest triboelectric effect, possibly due to its uniform coating around the copper wire (Figure 2F).

To enable tactile and sensing function in the embroidered button, some separation must be maintained between the top and bottom layers. The triboelectric signal increases with separation distance until a maximum threshold is reached.[41] To create this needed separation between the layers, we used a different embroidery structure for each layer; namely, the straight and satin structures. The straight structure, resembling traditional sewing, tightly affixes the yarn to the fabric, while the satin structure can suspend the yarn above the fabric (Figure S2). Given the greater strength and durability of the copper wire conductive yarn with a double-layer polyester and PU coating, it is used as the top layer, but its lack of flexibility causes it to remain close to the bottom layer even with the satin embroidery structure. To create extra space for separation and enhance triboelectric output, we placed spacers (a piece of cardboard) on straight embroidery with heights of 1 mm, 2 mm, and 3 mm during satin structure embroidery and removed it when embroidery was finished (Figures 1E, 3A, S3, and S4). The addition of spacers allows more yarn to occupy the same embroidery path, creating an overall arched shape.

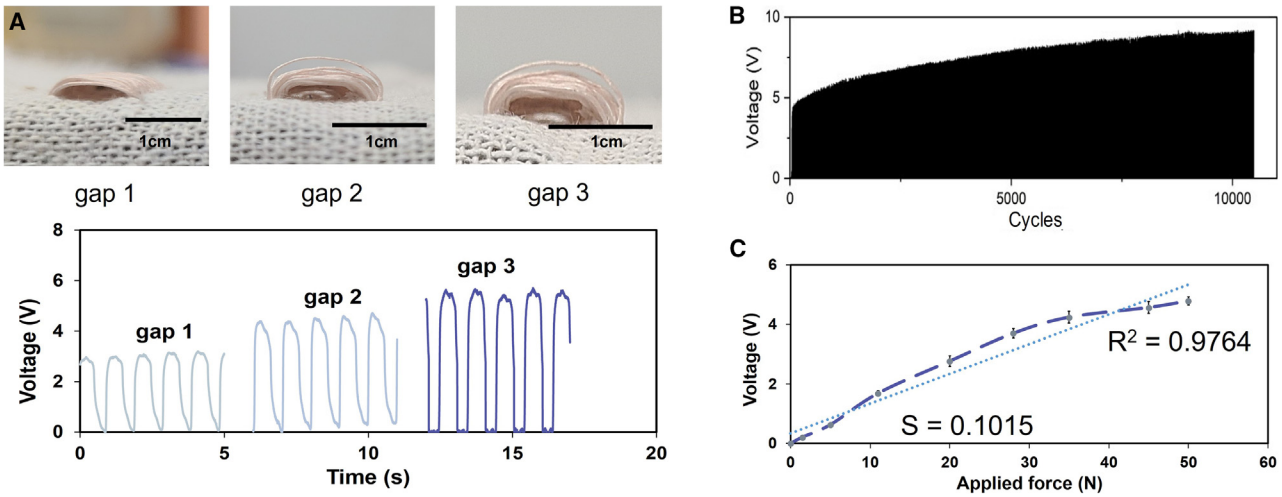

Figure 3. 3D embroidery characterization

(A) Embroidery with different "gaps" and their corresponding triboelectric performance.

(B) Durability test of the embroidered sensor under 40 N.

(C) Relationship between applied pressure and open-circuit voltage of the embroidered sensor.

The size of the embroidered sensor we tested is about 1 cm × 1.5 cm. The size of the bottom structure with PVDF-TrFE nano-microfiber wrapped yarn is about 0.6 cm × 1 cm. Triboelectric tests revealed that increasing the spacer height from 1 mm to 3 mm led to an output voltage increase from 3 V to 6 V (Figure 3B). We also conducted finite element simulation using COMSOL to qualitative analyze the potential difference distributions during pressing for the 3 mm gap sample, and the results correlated with the open-circuit voltage values (Figure S5). For the embroidered sensor with a 3-mm gap, the spacing reduces and stabilizes to ~2 mm after 50 cycles of pressing with a force of 40 N (Figures S6A–S6E; Video S1). This phenomenon occurs due to the use of spacers during the embroidery process, which increases the spacing between yarns as well as the overall length of the embroidery yarn. Given that the total embroidery area remains constant, these additional yarns appear as bulges. The larger gap allows the two layers of yarns to better maintain their distance when not pressed while providing a better contact surface when the top layer is pressed, thus providing a more robust on/off triboelectric signal (Table S2).

To test for durability, the embroidered sensor was tested for over 10,000 cycles at about 1.2 Hz and under a pressure of 40 N (Figure 3C). Due to the nature of triboelectricity, the sample accumulated charge during repeated testing, which led to a continuous and gradual increase in triboelectric output as the tests proceeded. The initial output voltage, approximately 5 V, rose to around 9 V after 10,000 cycles. This charge accumulation, specific to cyclic use, dissipates when the sample is left at rest, adhering to the characteristics of the TENG. Figures 2I and S7 illustrate the effect of varying pressure on the triboelectric output of the embroidered sensor. We employed a Linmot actuator to apply pressure to the embroidered sensor from 0 up to 50 N, which encompasses most finger-pressing scenarios. The voltage output of the embroidered sensor responds somewhat linearly to pressure, with a slope of about 0.1015 V/N, which is sufficient for finger-press identification.[29]

Figures 4A and 4B present the results of the washing test conducted on the embroidered sensor. Samples were washed with water only and with water and detergent. The embroidery maintained its shape and integrity before and after washing. However, the washing process did affect the triboelectric properties. The triboelectric output of the embroidered sensor remained stable after washing with water but was notably decreased after being washed with detergent. This reduction could be attributed to the softener ingredients present in the detergents used. The surfactants present in softeners can adhere to the yarns during the washing process, weakening the triboelectric properties (Figure S8). In the abrasion test conducted using a Martindale abrasion tester, the embroidered sensor exhibited remarkable durability (Figure S9). Thanks to its robust double-layer polyester and PU coating structure, the outer yarn surface showed no discernible changes after undergoing 8,000 abrasion cycles, even as the base fabric displayed severe pilling and wear (Figure 4C).

Machine learning model for signal recognition

The circuit diagram of the wearable system is shown in Figure S10. The positive and negative poles of the embroidery structure are connected to a 1-GΩ resistor that is linked to the analog reading ports on the Arduino Nano ESP32. When users engage in touch interactions with the embroidered sensor, a potential difference arises across the resistor. The triboelectric signal can then be obtained by calculating the difference between the readings from the two ports. We tested the sensitivity of the embroidered sensor under this system using finger pressure. The results are similar to those from the previous Linmot actuator test. The signal read by the Arduino shows a linear change within a pressure range of 0–80 kPa with a sensitivity of ~0.0073 V/kPa (Figure S11).

Figure S12 illustrates the process of data preparation for machine learning model training. First, the Arduino chip collects

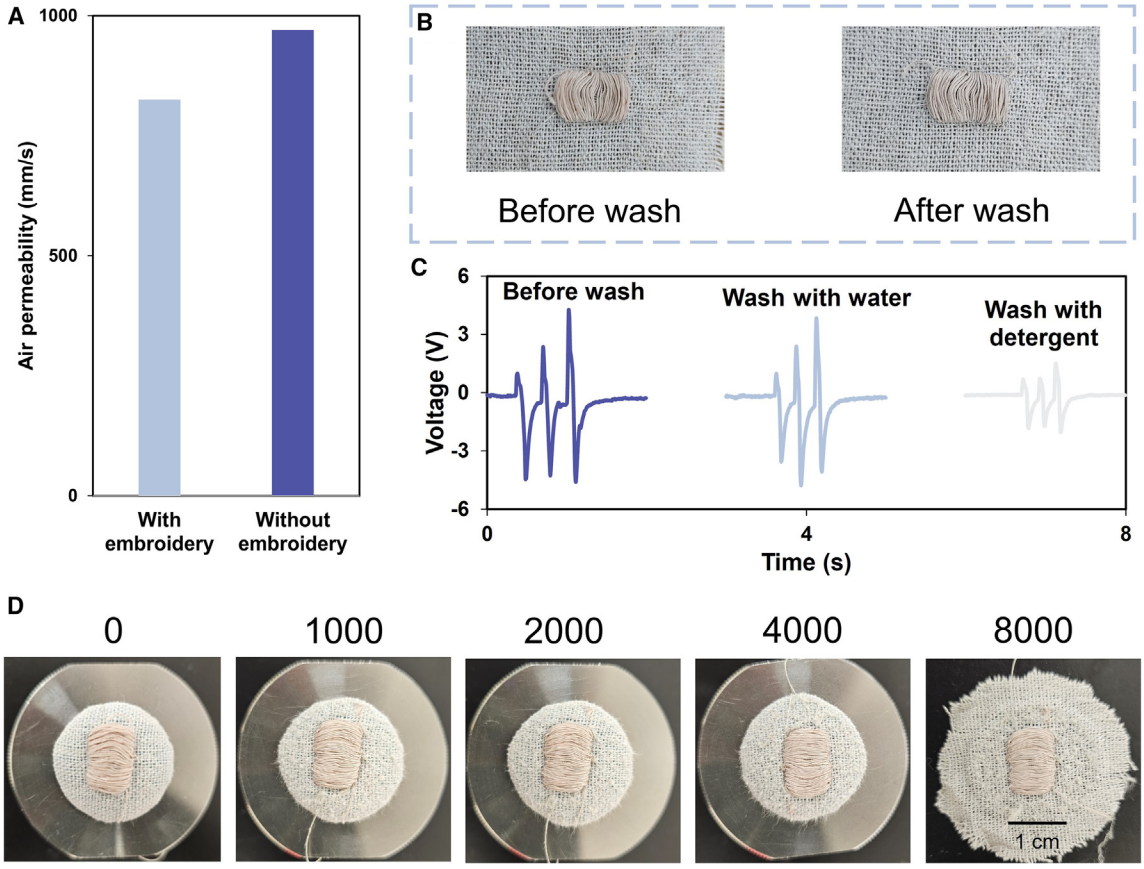

Figure 4. wearable TENG embroidered sensor

(A) Air permeability of the fabric with and without embroidery.

(B and C) Wash test of the embroidered sensor (B) and the corresponding change of the triboelectric signal before and after washing with water and detergent (C).

(D) Abrasion test of the embroidered sensor.

triboelectric signals generated by touch interactions (Figure 5A). Next, the collected data are labeled and prepared for supervised machine learning model training. When the chip receives a signal that exceeds the set threshold, it records the signal. To comprehensively capture all signals for one interaction, we configure the chip to record data both before and after the threshold is crossed. The original recorded signal undergoes digital amplification and filtering to yield high-quality data. All signal processing steps occur on the chip. After uploading the trained model to the microprocessor, the newly collected data are sent to the processing unit for touch interaction identification.

To optimize the algorithm selection, we tested a number of machine learning models and algorithms (Figure S13). Among them, the TensorFlow-based neural network supports 1D data input, which aligns well with TensorFlow Lite Micro, a machine learning database/library tailored to be run on microchips. Our experiments revealed that, when configuring neural network training parameters, the combination of multiple different activations/layers (such as elu, tanh, and leaky_relu) outperformed single activations. The final model achieved an accuracy rate of 99%, with errors occurring only in the recognition of the long press (Figure 5B).

Application demonstrations

To showcase its potential for interacting with wireless devices, we developed a music player mobile app that can be controlled using the embroidery button via Bluetooth. We designed six functions: "play/pause," "next song," "last song," "volume up," "volume down," and "mute," each linked to a specific gesture. Video S2 provides a demonstration of the music player app and the embroidered sensor by a volunteer.

Because of its high positive triboelectric performance from the PU coating, the embroidered button can also be activated without touching (Figure S14A). By applying a layer of Polytetrafluoroethylene (PTFE) tape to a nylon fabric, we create an electrostatic induction device. When the device—a finger cot—approaches the embroidered sensor, a positive electric signal is induced, followed by a negative electric induction signal when the finger cot is removed (Figures S14B–S14C). By detecting the presence of positive or negative peaks exceeding a defined threshold, we can employ the embroidered sensor as a binary switch to turn the music player app on or off, but without touching (Figure S14D; Video S3).

To enable more complex interactions, we combined two embroidered sensors with different "gaps" to create a

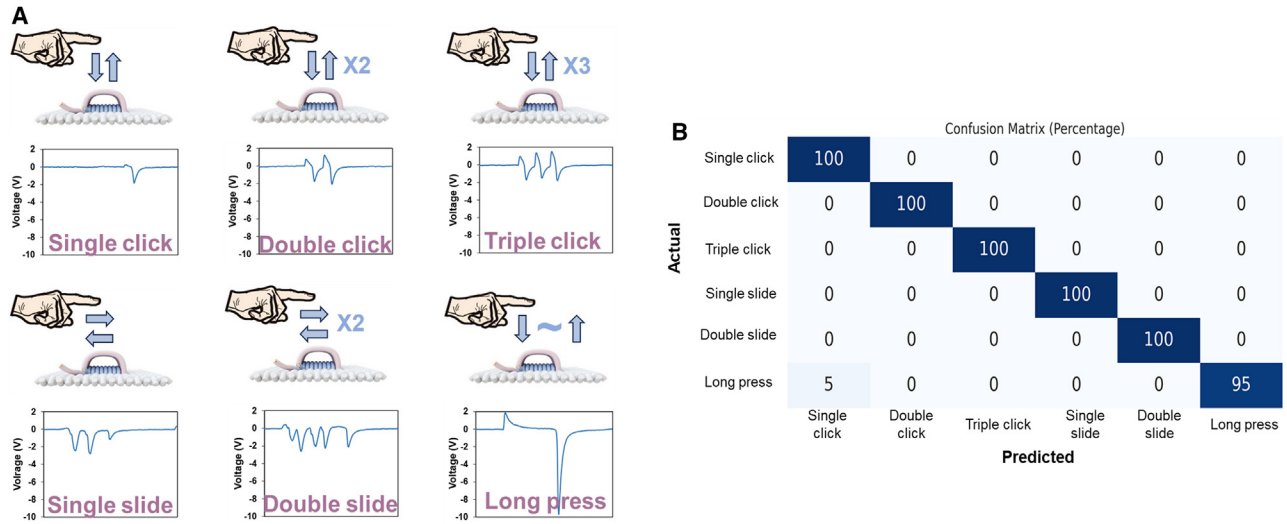

Figure 5. Deep-learning-assisted TENG embroidered sensor for human-machine interaction

(A) Demonstration of the embroidered sensor controlling the music player app, including the interaction ways and corresponding signals.

(B) The confusion matrix of the neural network model with multiple different activation combinations.

dual-channel textile-computer interaction sensor (Figures 6A and S15). Figure 6B shows that the peak value from the sensor with the 3-mm gap is higher than the peak value from the sensor with the 1-mm gap. The 3 mm + 1 mm dual sensor supports two-finger operation, providing a wider range of combinations and variations. Additionally, the introduction of varying gaps increases the disparity between the input signals of the two sensors, enhancing signal classification accuracy for more complex gestures and gesture combinations.

Figure S16A and Video S4 demonstrate the application of the two sensors in gesture-based password setting and input. Here, the password was set to mimic the famous "Konami code" commonly appearing in video games. In this scenario, the password execution is defined as follows: sliding twice on the right sensor, clicking the left sensor, clicking the right sensor, clicking the left sensor, clicking the right sensor, long pressing on the right sensor, and finally pressing both sensors simultaneously. For password program settings, we selected nine feature values as the basis for password verification (Figure S16B). The password input is limited to a time window of 7 s. During password setting, the user is tasked to input the desired sequence of inputs on the embroidered sensor 10 times, and the program calculates the average of the aforementioned feature values. During password verification, the program analyzes the input signals and confirms correct password entry if all of the nine measured feature values fall within 25% of the value during password setting.

The dual-sensor design significantly expands the complexity of interactions and is applicable to more intricate programs, such as game control. In total, we designed 17 distinct touch interactions on the embroidered sensor, corresponding to the game's keyboard inputs and key combinations, including simple sequences and durations of clicks, slides, presses, etc. (see Figure S17 for more details) After processing by the machine learning model, clear boundaries emerge, signifying the model's strong data classification capability with nearly 100% accuracy in classification of the 17 interactions (Figure S18). Video S5 demonstrates game control using this sensor and machine learning model. Figure S17D displays typical triboelectric signal values corresponding to different keys and their operations in the game. The selection of the 17 keys was based on the selected game's specific input requirements and can be adapted for more or fewer types of interaction as needed.

To further test more complex designs using the embroidered sensors, we created and tested a sensing array for recognizing object shapes and materials (Figures 7A, 7B, and S19). Figures 7C–7E illustrate the contrasting triboelectric signals produced by nylon (a strongly positive triboelectric material) and PTFE (a strongly negative triboelectric material) as well as the distinctions in signals generated by silk (a weakly positive triboelectric material) and polyester (a weakly negative triboelectric material) (Figure S20). In pursuit of simultaneously recognizing object shapes and materials, we constructed a 4 × 4 matrix (4 cm × 4 cm) and incorporated machine learning for classification (Figure 7F). Employing the same signal acquisition and machine learning methodologies as before, we gathered signals from three different shapes (square, circle, and triangle) and four different materials (nylon, silk, polyester, and PTFE). The rectangle we used was 2.5 cm (length) × 2 cm (width). The diameter of the circle was ~2.5 cm. The length of triangle was ~4 cm, and the height was ~3 cm. These signals were then divided into two groups for machine learning classification, considering the materials and shapes of different objects. The collected data were labeled and divided into three groups based on shape for training and four groups based on material for training. The results, as depicted in Figures 7G and 7H, indicate an accuracy of 98% in material identification and 92% in shape recognition. This discrepancy may arise from electrostatic induction generating signals in addition to those produced by direct contact.

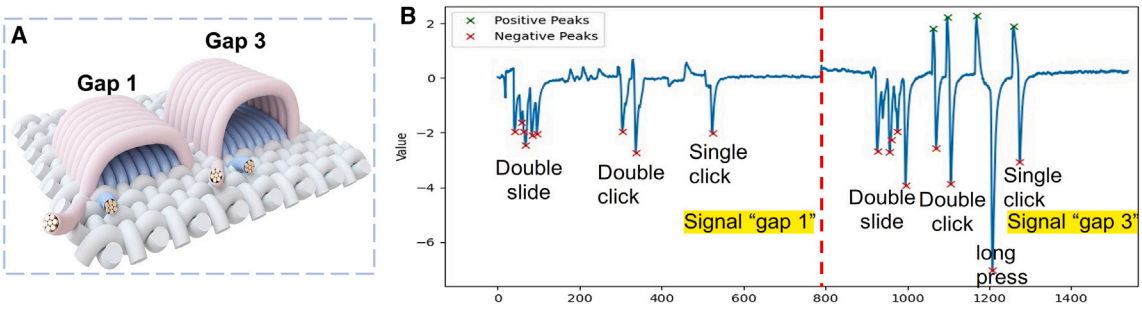

Figure 6. Application demonstrations of the dual-channel embroidered sensor

(A) A dual-channel embroidered sensor with different "gaps."

(B) Signal plot from password setting.

Conclusion and outlook

In this work, we used embroidery to integrate two conductive yarns with opposite triboelectric properties into textile fabric and created a "clickable" and self-powered triboelectric button. Using different embroidery structures, we optimized the gap size between the two embroidered layers. The resulting embroidered sensor demonstrates a linear response up to at least 50 N and exhibits exceptional durability. We employed machine learning for recognizing single inputs and input combinations. By combining two embroidered sensors with different gap sizes, we created a dual-sensor device that allows for more complex inputs, showcasing their potential for applications such as password setting and game control. As a self-powered sensor, this technology fulfills the stringent requirements of smart textiles, boasting low power consumption, ease of integration, and an imperceptible presence. Its deployment significantly enhances user experience in daily interactions with smart devices. However, the whole system showed significant delay, which may come from the limited computing power of the chips, the interference of Bluetooth LE and Python, and poor Bluetooth Low Energy (BLE) support. Follow-up research can focus on the optimization of wearable systems and hardware to provide a better user experience.

We also created a triboelectric embroidery matrix for object recognition and interaction that allows simultaneous identification of materials and shapes. This idea is still in its early stages. Existing embroidery technology cannot well complete an embroidery matrix composed of multiple monomers, and the resolution of the matrix is limited by the thickness of the yarn used.

EXPERIMENTAL PROCEDURES

Resource availability

Lead contact

Requests for further information, data, and resources will be fulfilled by the lead contact, Rong Yin (ryin@ncsu.edu).

Materials availability

PVDF-TrFE powder (70/30 mol %) was purchased from Piezo Tech (France). Ethyl acetate was purchased from Sigma-Aldrich. Silver-coated nylon conductive yarns were purchased from SwicoFill. The nylon conductive yarn from SwicoFill has a two-ply structure with plasma-coated silver. Its linear density is 315 D, its diameter is 0.21 mm, and its resistance is 51 Ω/m. PU-coated polyester-copper yarn was purchased from Volt (USA). Its linear density is 1318 D, its diameter is 0.34 mm, and its resistance is 3.57 Ω/m. Arduino chips were purchased from Arduino (USA).

Data and code availability

All programs were designed using the Arduino IDE and PyCharm. Specific code is available on GitHub (https://github.com/ychen242/AI-embroidery.git). Additional data and code are available from the lead contact, Rong Yin (ryin@ncsu.edu), upon request.

The fabrication of PVDF-TrFE nano-microfiber mats and nano-microfiber-wrapped yarn

The PVDF-TrFE nano-microfiber-wrapped yarn was produced using an airflow-driven system. This system was composed of a commercial airbrushing machine (1/3 HP, Master Airbrush Model TC-848) and a vortex tube. To perform solution blow spinning of the PVDF-TrFE nano-microfibers, the PVDF-TrFE powder was dissolved in ethyl acetate at room temperature for 1 day to prepare PVDF-TrFE solution (6% wt). Then, the PVDF-TrFE solution was transferred into the tank of the airbrushing gun (Master Airbrush G22 Model, 0.5-mm nozzle). The gas pressure for the airbrushing machine was controlled at approximately 60 psi. The distance between the airbrushing gun and the collector was approximately 15 cm. After nano-microfiber collection, it was transferred into an oven at 60°C for 1 h of drying. Finally, the embroidery sample was embroidered onto cloth or other textiles.

Embroidered sensor fabrication

The embroidery was achieved using a Tajima embroidery machine. First, the PVDF-TrFE nano-microfiber-wrapped yarn was embroidered onto cotton fabric using a default "straight" structure. Then, three spacers (a piece of hard object) with different heights (1 mm, 2 mm, 3 mm) were attached on the PVDF-TrFE nano-microfiber-wrapped yarn embroidery. Finally, the PU-coated polyester-copper yarn was embroidered along the spacer using the "satin" structure. After embroidery, the spacer was removed, and the sample was washed for 30 min and dried at 80°C for 1 h.

Characterization and measurement

Surface morphology analysis was conducted using a Hitachi TM4000II SEM with an accelerating voltage of 15 kV and a detector setting that combined mixed secondary electrons and backscattering electrons.

Mechanical performance test

Mechanical testing was conducted using an MTS Q-Test tensile tester (Instron 5567). The tensile tester followed the guidelines outlined in ASTM D2256, recording the break strength (gf) and strain at break (percent) for each sample.

Triboelectric performance test and durability test

The test frequency was 1.2 Hz unless noted otherwise. The electrical output performance was recorded using an electrometer (Keithley 6514). A linear mechanical motor (LinMot E1100) was used to provide contact and separation between the friction material and the test sample and to control the influencing factors during measurement. The signal was transferred from the measuring system to the computer via a data acquisition (DAQ) card.

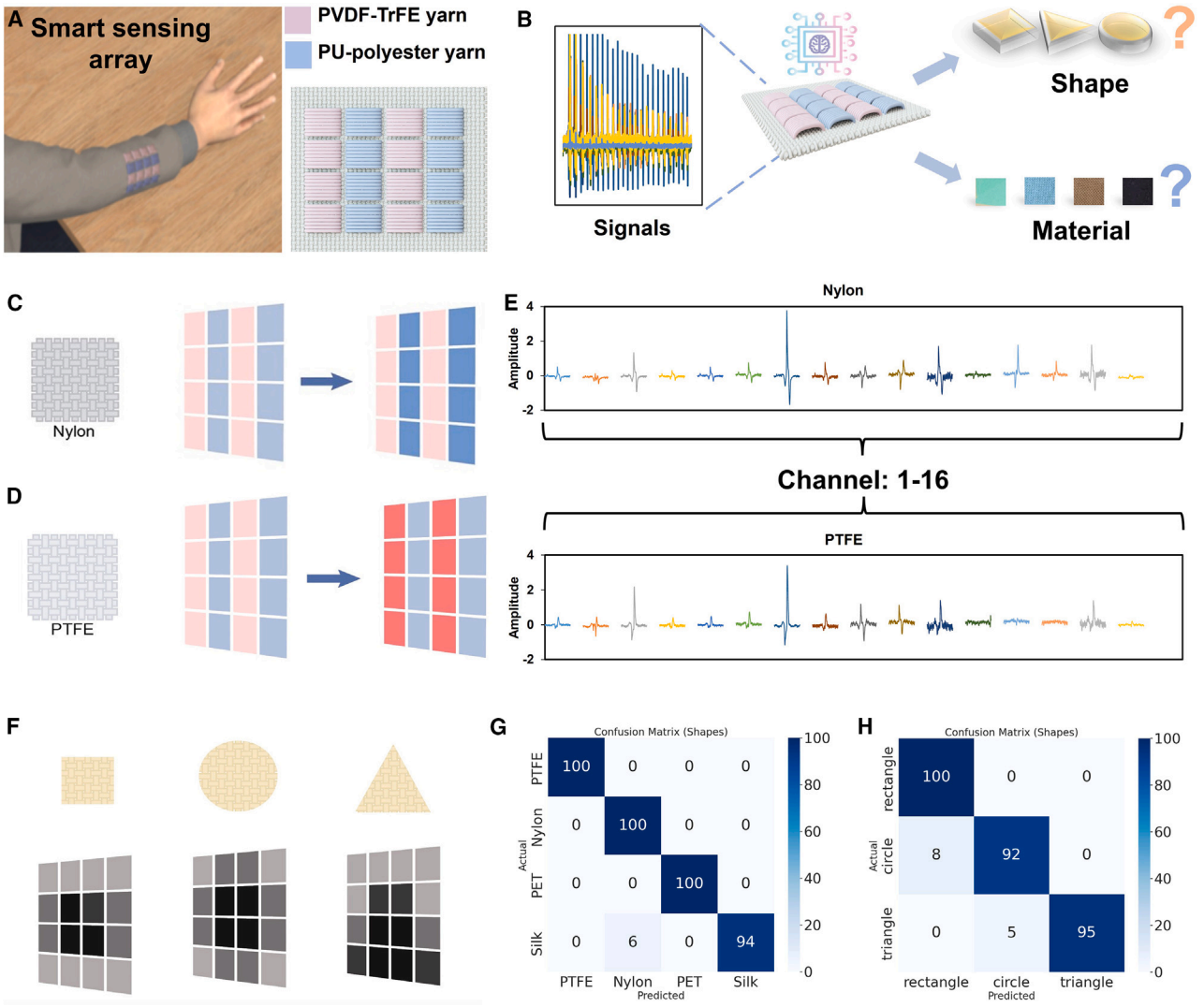

Figure 7. Smart sensing array fabricated by embroidery for object interaction

(A and B) Schematics of the embroidery sensing array.

(C and D) Sensing and recognition of the embroidery sensing array based on different materials of objects (nylon and PTFE).

(E) Signals produced by nylon and PTFE when in contacted with the embroidery sensing array.

(F) Sensing and recognition of the embroidery sensing array based on different shapes of objects.

(G) Confusion matrix results of the trained model for material identification.

(H) Confusion matrix results of the trained model for shape identification.

The deformation and potential distribution simulation of the embroidery sample

To gain a clearer understanding of the working mechanism of the cored yarn, COMSOL finite element simulation was used to qualitatively analyze the potential difference and corresponding deformation. We placed eight conductive yarns wrapped in PVDF-TrFE evenly on a cotton cloth substrate as a lower plate. We set the thickness to 0.2 mm and the width to 8 mm and set the lower plate as a fixed constraint. We set the PU-coated copper wire as an arch with a coating thickness of 0.1mm, fixed the two ends of the arch, and simulated the downward squeezing motion of fingers at the arch's position. We applied a sinusoidal motion with an amplitude of 1 mm/2 mm/3 mm and a frequency of 1.4 Hz. The material for the topside yarn was a PU coating with a surface charge density of 0.6 μCm^2 and permittivity values of 5. The material for the bottom side yarn was PVDF-TrFE with a surface charge density of 0.6 μCm^2 and permittivity values of 9.3. Air filled the remaining space and set the outer layer to ground as an infinite cell domain.

Air permeability measurement

An embroidery sample was fixed on the surface of the air permeability tester's opening (Air Permeability Tester RH-TQZ500). The test area was 10 cm^2, and the test unit was millimeters per second, according to ISO 9237. A vacuum pump was used to provide a stable airflow to maintain the air pressure difference (ΔP) at 100 Pa between the upper and lower areas of the sample.

Washing test

Two embroidery samples were separately washed in a beaker with pure water or aqueous detergent solution (1 mg/mL) for 30 min with a magnetic rotator.

Then the sample was dried in an oven at 80°C for 1 h. This process was repeated 5 times.

Abrasion test

The abrasion resistance was evaluated according to ASTM D4966 using an SDL Atlas Martindale abrasion tester. A 4 × 4 cm embroidery sample was used for the abrasion test. Fixed weights were loaded to apply 9-kPa pressure on each sample. A picture was taken every 1,000 cycles to evaluate the abrasion resistance.

Design of the music player app on Android, touchless interaction program, password setting program, and game control program

The music player app was developed using Android Studio. It has a function that can scan nearby BLE devices and connect with them. It can also receive data from a BLE device and convert it to a string. When a specific string is received (e.g., single click, double click, etc.), it triggers corresponding functions, such as play/pause and change music, which are shown on the user interface.

Data collection

For the music player app, we used a total of 600 samples consisting of 100 samples for each of the 6 interactive signals. These samples were then augmented using a data augmentation program, resulting in a dataset of 1,200 samples to be used for training the finalized machine learning parameters. The training data size was 70%, the testing data size was 15%, and 15% was used for validation. The sample was collected 0.6 s before threshold detection and 1.1 s after threshold detection. The device's sampling frequency was set to 1 ms, averaging every 10 data points, with 180 data points per sample.

For game control, the dataset comprised 1,020 samples initially, with 60 samples collected for each of the 17 interactive signals. Through the data augmentation process, these samples were expanded to 2,040, ensuring a comprehensive dataset for training the machine learning parameters. The training data size was 70%, the testing data size was 15%, and 15% was used for validation. The sample was collected 0.3 s before threshold detection and 1 s after threshold detection. The device's sampling frequency was set to 1 ms, averaging every 10 data points, with 130 data points per channel and a total of 260 data points for each sample.

SUPPLEMENTAL INFORMATION

Supplemental information can be found online at https://doi.org/10.1016/j.device.2024.100355.

ACKNOWLEDGMENTS

This work was supported by the Wilson College Strategic Collaborative Research & Innovation Fund (SCRIF) at NCSU. Y. Ling acknowledges financial support from the VF Graduate Student Impact Award. Y.Y. acknowledges financial support from the Provost's Doctoral Fellowship and Goodnight Doctoral Fellowship at NCSU. We thank Shubham Kakirde for assistance with developing the music player app on Android.

AUTHOR CONTRIBUTIONS

Y.C., methodology, formal analysis, investigation, and writing – original draft; Y. Ling., visualization and investigation; Y.Y., formal analysis; Z.W., software, investigation, and writing – original draft; Y. Liu., writing – review & editing and project administration; B.Y., investigation and resources; W.G., resources; R.Y., conceptualization, writing – review & editing, supervision, and funding acquisition.

DECLARATION OF INTERESTS

The authors declare no competing interests.

Received: January 19, 2024
Revised: February 4, 2024
Accepted: March 15, 2024
Published: April 12, 2024

REFERENCES

1. Zhou, X., Wang, Z., Xiong, T., He, B., Wang, Z., Zhang, H., Hu, D., Liu, Y., Yang, C., Li, Q., et al. (2023). Fiber Crossbars: An Emerging Architecture of Smart Electronic Textiles. Adv. Mater., e2300576. https://doi.org/10.1002/adma.202300576.
2. Chen, Y., Hart, J., Suh, M., Mathur, K., and Yin, R. (2023). Electromechanical Characterization of Commercial Conductive Yarns for E-Textiles. Textiles *3*, 294–306. https://doi.org/10.103390/textiles3030020.
3. Ling, Y., Hart, J., Henson, C., West, A., Kumar, A., Karanjikar, M., and Yin, R. (2023). Investigation of Hemp and Nylon Blended Long-Staple Yarns and Their Woven Fabrics. Fibers Polym. *24*, 1835–1843. https://doi.org/10.1007/s12221-023-00180-1.
4. Liu, X., Chen, G., Bao, J., and Xu, X. (2022). General Preparation and Shaping of Multifunctional Nanowire Aerogels for Pressure/Gas/Photo-Sensing. Adv. Fiber Mater. *4*, 66–75. https://doi.org/10.1007/s42765-021-00076-w.
5. Ma, S., Wang, X., Li, P., Yao, N., Xiao, J., Liu, H., Zhang, Z., Yu, L., Tao, G., Li, X., et al. (2022). Optical Micro/Nano Fibers Enabled Smart Textiles for Human–Machine Interface. Adv. Fiber Mater. *4*, 1108–1117. https://doi.org/10.1007/s42765-022-00163-6.
6. Wang, R., Du, Z., Xia, Z., Liu, J., Li, P., Wu, Z., Yue, Y., Xiang, Y., Meng, J., Liu, D., et al. (2022). Magnetoelectrical Clothing Generator for High-Performance Transduction from Biomechanical Energy to Electricity. Adv. Funct. Mater. *32*, 2107682, n/a. https://doi.org/10.1002/adfm.202107682.
7. Chen, W.Q., Zhang, X.Y., Li, P., Gharavi, H., Hao, Y., Ouyang, J., Hu, J., Hu, L., Hou, C., Humar, I., et al. (2022). Fabric computing: Concepts, opportunities, and challenges. Innovation *44*, 3, 10.10340. https://doi.org/10.1016/j.xinn.2022.100340.
8. Chen, M., Jiang, Y., Guizani, N., Zhou, J., Tao, G., Yin, J., and Hwang, K. (2020). Living with I-Fabric: Smart Living Powered by Intelligent Fabric and Deep Analytics. NET-M *34*, 156–163. https://doi.org/10.1109/MNET.011.1900570.
9. Smith, M., Cacucciolo, V., and Shea, H. (2023). Fiber pumps for wearable fluidic systems. Science *379*, 1327–1332.
10. Chen, Y., Yang, Y., Li, M., Chen, E., Mu, W., Fisher, R., and Yin, R. (2021). Wearable Actuators: An Overview, Textiles (Basel), *1*, pp. 283–321. https://doi.org/10.103390/textiles1020015.
11. Yi, J., Dong, K., Shen, S., Jiang, Y., Peng, X., Ye, C., and Wang, Z.L. (2021). Fully Fabric-Based Triboelectric Nanogenerators as Self-Powered Human–Machine Interactive Keyboards. Nano-Micro Lett., 13, 10.103. https://doi.org/10.1007/s40820-021-00621-7.
12. Lai, Y., Lu, H., Wu, H., Zhang, D., Yang, J., Ma, J., Shamsi, M., Vallem, V., and Dickey, M.D. (2021). Elastic Multifunctional Liquid–Metal Fibers for Harvesting Mechanical and Electromagnetic Energy and as Self-Powered Sensors. Adv. Energy Mater. *11*, 11.n/a. https://doi.org/10.1002/aenm.202100411.
13. Niu, L., Peng, X., Chen, L., Liu, Q., Wang, T., Dong, K., Pan, H., Cong, H., Liu, G., Jiang, G., et al. (2022). Industrial production of bionic scales knitting fabric-based triboelectric nanogenerator for outdoor rescue and human protection. Nano Energy, 97, 10.107168. https://doi.org/10.1016/j.nanoen.2022.107168.
14. Ma, Y., Ouyang, J., Raza, T., Li, P., Jian, A., Li, Z., Liu, H., Chen, M., Zhang, X., Qu, L., et al. (2021). Flexible all-textile dual tactile-tension sensors for monitoring athletic motion during taekwondo. Nano Energy, 85. https://doi.org/10.1016/j.nanoen.2021.105941.
15. Zhu, D., Zhang, Z., Chen, M., Li, P., Xiang, Y., Ouyang, J., Huang, Z., Liu, X., Wang, F., Yang, M., et al. (2023). A Perspective on Rhythmic

Gymnastics Performance Analysis Powered by Intelligent Fabric. Adv. Fiber Mater. *5*, 1–1110. https://doi.org/10.1007/s42765-022-00197-w.

16. Guan, F., Xie, Y., Wu, H., Meng, Y., Shi, Y., Gao, M., Zhang, Z., Chen, S., Chen, Y., Wang, H., and Pei, Q. (2020). Silver Nanowire–Bacterial Cellulose Composite Fiber-Based Sensor for Highly Sensitive Detection of Pressure and Proximity. ACS Nano *14*, 15428–15439.
17. Zhang, Q., Wang, Y.L., Xia, Y., Zhang, P.F., Kirk, T.V., and Chen, X.D. (2019). Textile-Only Capacitive Sensors for Facile Fabric Integration without Compromise of Wearability. Adv. Mater. Technol. *4*, 4.n/a. https://doi.org/10.1002/admt.201900485.
18. Zhong, J., Ma, Y., Song, Y., Zhong, Q., Chu, Y., Karakurt, I., Bogy, D.B., and Lin, L. (2019). A Flexible Piezoelectret Actuator/Sensor Patch for Mechanical Human–Machine Interfaces. ACS Nano *13*, 7107–7116.
19. Xu, Q., Wang, Z., Zhong, J., Yan, M., Zhao, S., Gong, J., Feng, K., Zhang, J., Zhou, K., Xie, J., et al. (2023). Construction of Flexible Piezoceramic Array with Ultrahigh Piezoelectricity via a Hierarchical Design Strategy. Adv. Funct. Mater. *33*. https://doi.org/10.1002/adfm.202304402.
20. Luo, Y., Wang, Z., Wang, J., Xiao, X., Li, Q., Ding, W., and Fu, H.Y. (2021). Triboelectric bending sensor based smart glove towards intuitive multi-dimensional human-machine interfaces. Nano Energy *89*, 10.106330. https://doi.org/10.1016/j.nanoen.2021.106330.
21. Wen, F., Sun, Z., He, T., Shi, Q., Zhu, M., Zhang, Z., Li, L., Zhang, T., and Lee, C. (2020). Machine Learning Glove Using Self-Powered Conductive Superhydrophobic Triboelectric Textile for Gesture Recognition in VR/AR Applications. Adv. Sci. *7*, 2000261-n/a. https://doi.org/10.1002/advs.202000261.
22. Fang, H., Wang, L., Fu, Z., Xu, L., Guo, W., Huang, J., Wang, Z.L., and Wu, H. (2023). Anatomically Designed Triboelectric Wristbands with Adaptive Accelerated Learning for Human–Machine Interfaces. Adv. Sci. *10*, e2205960-n/a. https://doi.org/10.1002/advs.202205960.
23. Tan, P., Han, X., Zou, Y., Qu, X., Xue, J., Li, T., Wang, Y., Luo, R., Cui, X., Xi, Y., et al. (2022). Self-Powered Gesture Recognition Wristband Enabled by Machine Learning for Full Keyboard and Multicommand Input. Adv. Mater. *34*, e2200793-n/a. https://doi.org/10.1002/adma.202200793.
24. Liu, Y., Yiu, C., Song, Z., Huang, Y., Yao, K., Wong, T., Zhou, J., Zhao, L., Huang, X., Nejad, S.K., et al. (2022). Electronic skin as wireless human-machine interfaces for robotic VR. Science advances *8*, eabl6700. https://doi.org/10.1126/sciadv.abl6700.
25. Pratap, A., Gogurla, N., and Kim, S. (2022). Elastic and Skin-Contact Triboelectric Nanogenerators and Their Applicability in Energy Harvesting and Tactile Sensing. ACS Appl. Electron. Mater. *4*, 1124–1131. https://doi.org/10.1021/acsaelm.1c01246.
26. Xu, J., Tat, T., Zhao, X., Zhou, Y., Ngo, D., Xiao, X., and Chen, J. (2022). A programmable magnetoelastic sensor array for self-powered human–machine interface. Appl. Phys. Rev. *9*. https://doi.org/10.1063/5.0094289.
27. Fang, D., Ding, S., Dai, Z., Zhong, J., and Zhou, B. (2023). Wearable patch with direction-aware sensitivity of in-plane force for self-powered and single communication channel based human-machine interaction. Chem. Eng. J. *1996*, 468. https://doi.org/10.1016/j.cej.2023.143664.
28. Dong, K., Peng, X., An, J., Wang, A.C., Luo, J., Sun, B., Wang, J., and Wang, Z.L. (2020). Shape adaptable and highly resilient 3D braided triboelectric nanogenerators as e-textiles for power and sensing. Nat. Commun. *11*, 2868. https://doi.org/10.1038/s41467-020-16642-6.
29. Chen, Y., Ouyang, J., Shang, L., Li, B., Li, J., Hao, Y., Gong, Y., Hu, J., Zhou, J., Wang, R., et al. (2022). Imperceptible, designable, and scalable braided electronic cord. Int. J. Biol. Macromol. *220*, 13–21, 7097. https://doi.org/10.1038/s41467-022-34918-x.
30. Chen, Y., Ling, Y., and Yin, R. (2022). Fiber/yarn-based triboelectric nanogenerators (TENGs): fabrication strategy, structure, and application. Sensors, 22. https://doi.org/10.3390/s22249716.
31. Dong, K., Peng, X., and Wang, Z.L. (2020). Fiber/Fabric-Based Piezoelectric and Triboelectric Nanogenerators for Flexible/Stretchable and Wearable Electronics and Artificial Intelligence. Adv. Mater. *32*, e1902549-n/a. https://doi.org/10.1002/adma.201902549.
32. Chen, Y., Chen, E., Wang, Z., Ling, Y., Fisher, R., Li, M., Hart, J., Mu, W., Gao, W., Tao, X., et al. (2022). Flexible, durable, and washable triboelectric yarn and embroidery for self-powered sensing and human-machine interaction. Nano Energy, 104. https://doi.org/10.1016/j.nanoen.2022.107929.
33. Yan, D., Ye, J., Zhou, Y., Lei, X., Deng, B., and Xu, W. (2023). Research Progress of Fabrics with Different Geometric Structures for Triboelectric Nanogenerators in Flexible and Wearable Electronics. Adv. Fiber Mater. *5*, 1852–1878. https://doi.org/10.1007/s42765-023-00334-z.
34. Ye, C., Yang, S., Ren, J., Dong, S., Cao, L., Pei, Y., and Ling, S. (2022). Electroassisted Core-Spun Triboelectric Nanogenerator Fabrics for IntelliSense and Artificial Intelligence Perception. ACS Nano *16*, 4415–4425. https://doi.org/10.1021/acsnano.1c10680.
35. Li, Y., Zhang, Y., Yi, J., Peng, X., Cheng, R., Ning, C., Sheng, F., Wang, S., Dong, K., and Wang, Z.L. (2022). Large-scale Fabrication of Core-shell Triboelectric Braided Fibers and Power Textiles for Energy Harvesting and Plantar Pressure Monitoring (EcoMat), 4 n/a. https://doi.org/10.1002/eom2.12191.
36. Ning, C., Tian, L., Zhao, X., Xiang, S., Tang, Y., Liang, E., and Mao, Y. (2018). Washable textile-structured single-electrode triboelectric nanogenerator for self-powered wearable electronics. J. Mater. Chem. A Mater. *6*, 19143–19150.
37. Ye, C., Dong, S., Ren, J., and Ling, S. (2020). Ultrastable and High-Performance Silk Energy Harvesting Textiles. Nano-Micro Lett. *12*, 43. https://doi.org/10.1007/s40820-019-0348-z.
38. Pyo, S., Kim, M., Kwon, D., Kim, W., Yang, J., Cho, H.S., Lee, J.H., and Kim, J. (2020). All-textile wearable triboelectric nanogenerator using pile-embroidered fibers for enhancing output power. Smart Mater. Struct. *29*, 055026. https://doi.org/10.1088/1361-665X/ab710a.
39. Ning, C., Wei, C., Sheng, F., Cheng, R., Li, Y., Zheng, G., Dong, K., and Wang, Z.L. (2023). Scalable one-step wet-spinning of triboelectric fibers for large-area power and sensing textiles. Nano Res. *16*, 7518–7526. https://doi.org/10.1007/s12274-022-5273-7.
40. Chen, Y., Hua, J., Ling, Y., Liu, Y., Chen, M., Ju, B., Gao, W., Mills, A., Tao, X., and Yin, R. (2023). An airflow-driven system for scalable production of nano-microfiber wrapped triboelectric yarns for wearable applications. Chem. Eng. J. https://doi.org/10.1016/j.cej.2023.147026.
41. Yang, B., Zeng, W., Peng, Z., Liu, S., Chen, K., and Tao, X. (2016). A fully verified theoretical analysis of contact-mode triboelectric nanogenerators as a wearable power source. Adv. Energy Mater. *6*, 1600505. https://doi.org/10.1002/aenm.201600505.